



HAL
open science

(93)Nb NMR spin echo spectroscopy in single crystal NbSe(3)

S. Suh, W.G. Clark, Pierre Monceau, R.E. Thorne, S.E. Brown

► **To cite this version:**

S. Suh, W.G. Clark, Pierre Monceau, R.E. Thorne, S.E. Brown. (93)Nb NMR spin echo spectroscopy in single crystal NbSe(3). *Physical Review Letters*, 2008, 101 (13), pp.136407. 10.1103/PhysRevLett.101.136407 . hal-00966731

HAL Id: hal-00966731

<https://hal.science/hal-00966731>

Submitted on 27 Mar 2014

HAL is a multi-disciplinary open access archive for the deposit and dissemination of scientific research documents, whether they are published or not. The documents may come from teaching and research institutions in France or abroad, or from public or private research centers.

L'archive ouverte pluridisciplinaire **HAL**, est destinée au dépôt et à la diffusion de documents scientifiques de niveau recherche, publiés ou non, émanant des établissements d'enseignement et de recherche français ou étrangers, des laboratoires publics ou privés.

^{93}Nb NMR Spin Echo Spectroscopy in Single Crystal NbSe_3 S. Suh,¹ W. G. Clark,¹ P. Monceau,² R. E. Thorne,³ and S. E. Brown¹¹*Department of Physics & Astronomy, UCLA, Los Angeles, California 90095-1547, USA*²*Institut Néel, CNRS/UJF, Grenoble, France*³*Department of Physics & Astronomy, Cornell University, Ithaca, New York 02222, USA*

(Received 28 July 2008; published 25 September 2008)

We report electric field induced phase displacements of the charge density wave (CDW) in a single crystal of NbSe_3 using ^{93}Nb NMR spin-echo spectroscopy. CDW polarizations in the pinned state induced by unipolar and bipolar pulses are linear and reversible up to at least $E = (0.96)E_T$. The polarizations have a broad distribution extending up to phase angles of order 60° for electric fields close to threshold. No evidence for polarizations in excess of a CDW wavelength or for a divergence in polarization near E_T are observed. The results are consistent with elastic depinning models, provided that the critical regime expected in large systems is not observable.

DOI: [10.1103/PhysRevLett.101.136407](https://doi.org/10.1103/PhysRevLett.101.136407)

PACS numbers: 71.45.Lr, 72.15.Nj, 74.70.Kn, 76.60.Cq

Depinning of bulk charge density waves above a threshold electric field E_T [1,2] is manifested in a variety of interesting collective transport phenomena, including nonlinear conductivity and coherent current oscillations [3]. In clean quasi-one-dimensional conductors such as NbSe_3 and $\text{K}_{0.3}\text{MoO}_3$, CDW pinning is very weak and E_T is, typically 0.1–100 mV/cm. In the pinned regime below E_T , these small depinning fields are associated with an enormous low-frequency polarizability and dielectric constants of 10^8 or more.

Many aspects of the pinned density wave response below E_T remain poorly understood. In models that treat the CDW as an extended periodic elastic medium pinned by disorder [4,5], depinning at E_T is considered a dynamic critical phenomenon [6–9], but what this might mean for the physical properties of systems such as CDWs remains a topic of current interest [10]. In the context of these models, as the ratio $f = (E - E_T)/E_T \rightarrow 0^-$, local CDW phase displacements occur in regions of increasing size, and the average displacement and polarization diverge according to $\chi \sim f^{-\gamma}$. Plasticity within rare regions of large CDW strain [11], or arising from additional terms in the equation of motion [12–14], could qualitatively change the behavior near E_T .

NMR spin-echo spectrometry provides a local probe of CDW polarizations, and can, in principle, examine the behavior near threshold and distinguish between elastic and plastic models. Here, we report NMR experiments on individual NbSe_3 crystals. We examine the temperature-dependent response of the CDWs that form below the two Peierls transitions ($T_{P1} = 144$ K, $T_{P2} = 59$ K), and focus on the response to current pulses at $T = 130$ K. The CDW polarization shows a nearly linear variation with E up to at least $(0.96)E_T$. The distribution of CDW displacements within the sample at this field is broad, with an average displacement of 22° and a width of 44° with no evidence for displacements larger than 1 CDW wavelength. These displacements are much larger than previously reported

[15,16] and are consistent with low-field dielectric measurements [2] and with elastic depinning models. However, the critical regime predicted by these models may be unobservable in a real CDW system.

NbSe_3 is the material of choice for studying CDW pinning and dynamics. Its whiskerlike morphology, crystal perfection and relatively small electronic anisotropy yield the most coherent collective response of any density wave or flux line lattice system [17]. Nuclear magnetic resonance spectroscopy is ideal for probing local CDW structure and dynamics in the presence of electric fields, and reveals bulk rather than surface or contact-related properties [15,16,18–20]. NMR spectroscopy combined with *in situ* transport measurements in NbSe_3 [15,16], in the blue bronze $\text{K}_{0.3}\text{MoO}_3$ [18,19], and in the spin-density wave compound $(\text{TMTSF})_2\text{PF}_6$ [21], have established that the density waves in these systems are incommensurate without discommensurations, and that the onset of nonlinear conduction at E_T corresponds to bulk CDW motion.

Previous NMR experiments on NbSe_3 have been hampered by weak signals because of the crystal size and morphology. Crystals have typical dimensions of $2 \mu\text{m}$ thick by $20 \mu\text{m}$ wide by a few mm long. As a result, both the number of ^{93}Nb nuclei within the NMR coil and its filling factor tend to be small. To obtain an adequate signal-to-noise ratio, Ross, Wang, and Slichter (RWS) [15,16] assembled a mosaic of crystals aligned along the whisker (**b**) axis and sharing common electrical contacts at each end. Accurately aligning the crystal axes orthogonal to (**b**) is challenging. RWS directed the magnetic field $\mathbf{B} \parallel \mathbf{b}$ to avoid complications from misalignment, but this gave a small filling factor. A more serious problem is that E_T is thickness dependent and varies between samples. By growing very large NbSe_3 single crystals and aligning the whisker axis along the coil axis so as to maximize the filling factor, we obtained ^{93}Nb NMR signals from an individual crystal. Two samples were examined and

yielded qualitatively and quantitatively similar results. All data presented here are for the second sample (S2), which was examined in more detail. S2 had a length of 12 mm, a width of 100 μm and a thickness of 11 μm (determined using the sample resistance from four-wire transport measurements with $\mathbf{I} \parallel \mathbf{b}$ and the sample resistivity $\rho = 0.19 \text{ m}\Omega \text{ cm}$ [22]). A coil of length 5 mm and inside diameter $\sim 130 \mu\text{m}$ was wound using 0.001" wire coated with Stycast 1266 epoxy for rigidity. Silver paste was used to form four electrical contacts between the sample and the printed circuit board on which it rested, with distances of $d_i = 8 \text{ mm}$ ($d_o = 10 \text{ mm}$) between the inner (outer) contacts. The low value of $E_T = 24 \text{ mV/cm}$ measured at $T = 130 \text{ K}$ indicates excellent crystal quality.

All of the ^{93}Nb NMR results presented here are for the central ($1/2, -1/2$) transition of this $I = 9/2$ nucleus. NbSe_3 has three distinct chains within its unit cell, and a distinct Nb site for each chain, named *yellow* (*y*), *orange* (*o*), and *red* (*r*) [15,23,24].

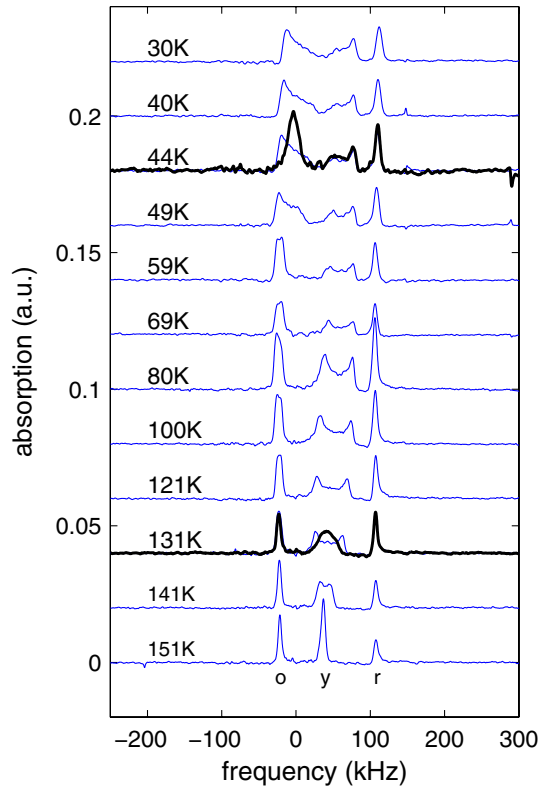


FIG. 1 (color online). Evolution of ^{93}Nb spectra [$I = (1/2, -1/2)$ transition] with temperature for an applied field $H_0 = 6.8 \text{ T}$. Formation of the \mathbf{Q}_1 CDW below $T_{P1} = 144 \text{ K}$ broadens and shifts the NMR line of the yellow (*y*) site [15,23,24]. Formation of the \mathbf{Q}_2 CDW below $T_{P2} = 59 \text{ K}$ most strongly affects the orange (*o*) site, and least the red (*r*) site. The heavy black curves represent spectra acquired at $T = 130 \text{ K}$ (44 K) with an applied electric field $E/E_T = 1.9$ (5.5) that depinned the \mathbf{Q}_1 (\mathbf{Q}_2) CDW.

The effects of CDW formation for $T < T_{P1}, T_{P2}$ on the Nb NMR spectrum are shown in Fig. 1. For $T > T_{P1}$, there are three sharp lines corresponding to the yellow, orange, and red chains. Rotating the magnetic field in the $\mathbf{a-c}$ plane yields spectral patterns for the yellow and orange sites that are qualitatively consistent with the normal state Knight shift and electric field gradient parameters reported by RWS [15]. An analysis of the relevant couplings to the CDWs will be described elsewhere [25].

Formation of the \mathbf{Q}_1 density wave below $T_{P1} = 144 \text{ K}$ most strongly affects the yellow site, and its spectrum is consistent with an incommensurate distortion, as noted previously [15,24]. We find that the resulting linewidth increases with magnetic field, at least for $H > 5 \text{ T}$ and a range of orientations [25]. From this, we conclude that the broadening from the \mathbf{Q}_1 CDW arises primarily via a modulation of the orbital part of the Knight shift. Effects related to nuclear electric quadrupolar coupling to the electric field gradient (EFG) also contribute to the line shape and width, but are less significant. In addition to a change in shape, the yellow peak's first moment shifts as T decreases below T_{P1} , due in part to the decrease in spin susceptibility associated with the CDWs [26]. Figure 2 shows how the linewidths ($\delta\nu$) and shifts ($\Delta\nu$) of the NMR peaks from the three Nb sites vary with temperature. The linewidth variation is compared with that of the CDW order parameter, determined from the square root of x-ray superlattice peak intensities (Δ, \circ) [27]. The yellow peak broadens as the temperature decreases below T_{P1} , but then narrows again at lower temperature. In contrast, the orange peak broadens

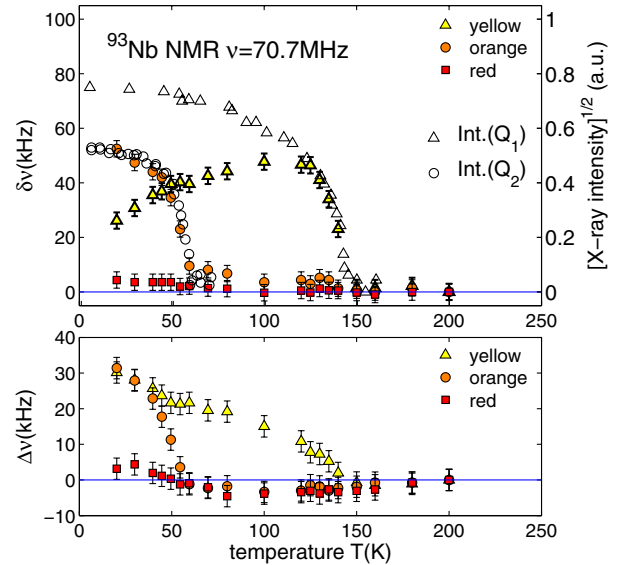


FIG. 2 (color online). Linewidths (*top*, $\delta\nu$) and frequency shifts (*bottom*, $\Delta\nu$) of the ^{93}Nb NMR central transition vs temperature, at angle $\alpha_{ac} = \pm 60^\circ$. A substantial fraction of the shift ($\Delta\nu$) for $T < T_{P1}, T_{P2}$ results from a decrease in spin susceptibility [26]. Open symbols (Δ, \circ) indicate the lattice modulation amplitude determined by x-ray diffraction [27].

continuously below T_{P2} , tracking the increase in the order parameter. The yellow peak's unexpected behavior may result from couplings (magnetic versus quadrupolar) of opposite sign, but further investigation is necessary. Following RWS, local phase (position) displacements of the CDW superlattice with respect to the underlying lattice in response to applied electric fields were probed using spin-echo measurements. As shown in the top right of Fig. 3, an electric field was applied along the chain (b) direction during all or part of the evolution time of the standard Hahn spin-echo sequence. If the CDW displaces in response to the field, the local environment of each ^{93}Nb nucleus will change by an amount that depends upon the coupling to the CDW and the magnitude of the local displacement. The echo is recorded as a function of the durations τ_1 and τ_2 during which $E \neq 0$. In most experiments, only a single electric field pulse was applied, with duration τ_1 .

The main panel of Fig. 3 shows the echo amplitude at $T = 130$ K as a function of the width τ_1 of an electric field pulse $E = (1/2)E_T$, for magnetic fields corresponding to the center (C) and the singular edge (E) of the yellow site (see spectrum, lower right). These decays are corrected for the background echo decay, which is Gaussian with a time scale $T_2 = 1$ ms. The inset at the lower left of Fig. 3 shows two echo decays for spectral component (C). In one (\circ), an E -field pulse of amplitude $E = (0.96)E_T$ (\circ) is applied

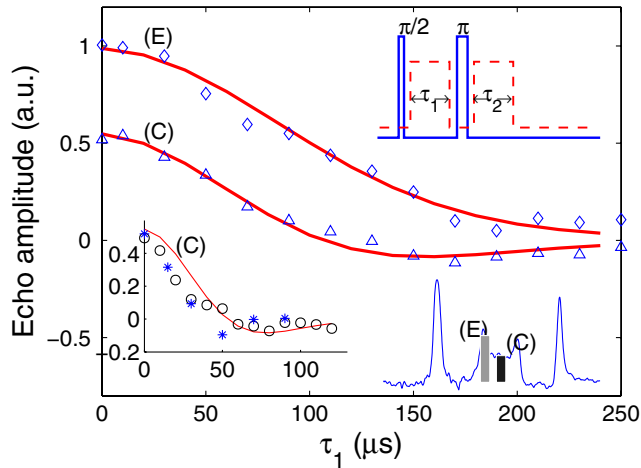


FIG. 3 (color online). *top right*: Hahn spin-echo sequence, labeled with times τ_1 , τ_2 , during which electric field pulses could be applied to displace the CDW phase. *bottom right*: Echo spectrum with labeled components of width 10 kHz near the center (C) and one edge (E) of the yellow peak. *main panel*: Echo decays in the presence of electric field pulses $E = (1/2)E_T$, measured at the center (C, \triangle) and edge (E, \diamond) of the yellow peak at $T = 130$ K. The solid lines are fits corresponding to the distribution of CDW phase displacements shown in Fig. 4. *lower left*: Same as main panel, but with $E = (0.96)E_T$ applied during τ_1 (\circ), and with $E = (1/2)E_T$ applied with opposite polarity during τ_1 and τ_2 (\star). The solid line matches the decay in the main panel, but with the time scale reduced by factor two.

during τ_1 . In the other (\star), two equal duration electric field pulses of magnitude $|E| = \frac{1}{2}E_T$ are applied with opposite polarity (\star) during τ_1 and τ_2 . If the CDW's phase displacement varies linearly with electric field, then doubling the magnitude of the field or applying pulses of opposite sign should double the displacement, and thus halve the echo decay time. The solid line is identical to the decay for (C) and $E = (1/2)E_T$ in the main panel, but with the time scale reduced by factor two. The agreement with the data strongly suggests a linear phase displacement response.

To interpret these results in more detail, we assume the CDW coupling to the Nb nuclei is magnetic, that the CDW lattice distortion at the i th nuclear site is $u_i(x_i) = u_0[\cos\{\mathbf{Q}_1 x_i + \phi(x_i)\}]$, and that the resulting frequency shift of the i th spin has the form

$$\delta\nu_i \propto du_i(x)/dx_i. \quad (1)$$

The spin-echo amplitude (A) is determined by evaluating

$$A = \sum_i \cos[\Phi_i], \quad (2)$$

with $\Phi_i = [\omega_{1i} - \omega_{2i}]\tau_1$. Here, ω_{1i} (ω_{2i}) is the spin precession frequency while the electric field pulse is (is not) applied, and τ_1 is defined as in Fig. 3. If $\omega_{1i} = \omega_{2i}$, there is no suppression of the echo. However, displacing the CDW during τ_1 but not τ_2 leads to $\omega_{1i} \neq \omega_{2i}$ and defocusing of the transverse spin precession. In that case,

$$\omega_{1i} - \omega_{2i} \propto \delta u_i, \quad (3)$$

with $\delta u_i \sim \frac{du(x_i)}{d\phi} \delta\phi_i$ for small CDW phase displacements $\delta\phi_i$.

If the phase displacements $\delta\phi_i$ at each site are the same throughout the sample, then the echo decays will exhibit pronounced oscillations. In Fig. 3, any evidence for oscillations is weak, and this requires a broad distribution of phase displacements. The smooth curves through the data points in Fig. 3 (main panel and bottom left) are generated from the distributions $P(\delta\phi_i)$ of phase displacements shown in Fig. 4.

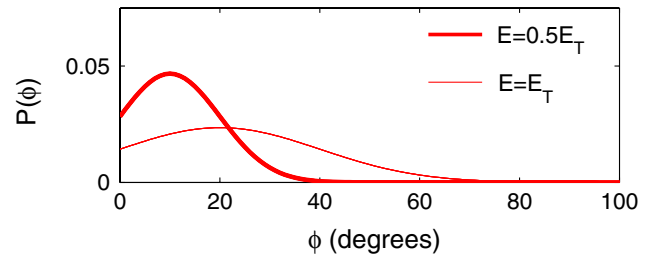


FIG. 4 (color online). The distribution of phase displacements used to generate the spin-echo decay curves (solid lines) in Fig. 3 (main panel), where $E = (1/2)E_T$ (bold line) and $E = E_T$ (thin line) is applied for duration τ_1 .

The data and fits shown in Fig. 3 demonstrate that the response is approximately linear with electric field for $E \leq E_T$. Doubling E from $0.5E_T$ to E_T or applying a bipolar pulse sequence with $|E| = 0.5E_T$ produces an echo that decays roughly twice as fast, corresponding to a phase displacement distribution with twice the mean value. The mean and width of the phase distribution are 10 and 22 deg at $E = 0.5E_T$ and 20 and 44 deg at $E = E_T$.

These values are much larger than the 2 deg displacement at $E = 0.75E_T$ reported by RWS [15]. The most likely cause of the difference is our use of a single crystal with a uniform cross section and sharp depinning threshold, rather than an aligned sample of multiple crystals with different thresholds. Although the displacements are relatively large, they are smaller than the 90 or 180 deg expected in a single coordinate model (depending upon the choice of pinning potential). The maximum phase displacement even for bipolar pulses is less than 90 deg. Displacements near threshold larger than 1 CDW wavelength (360 deg) have been predicted [28], but they may occur in too small a volume fraction to be detectable in our experiment.

The subthreshold CDW polarizations inferred from NMR can be compared to results from bulk transport measurements. Impurity pinning is responsible for both the threshold field E_T and the low-frequency dielectric constant ϵ_0 . In the single-particle model with a sinusoidal potential, the product $\epsilon_0 E_T = 4e\pi n_\perp$ with n_\perp the number of chains per unit area (SI units). For both CDWs in NbSe₃, the right side is $7.8(10)^9$ V/m. Transport experiments give 5×10^8 V/m (8×10^8 V/m for the Q_1 (Q_2) CDW [2]. The phase distribution obtained from echo decays combined with the measurement of E_T gives $1.5(10)^9$ V/m.

The present results show no evidence for diverging polarizations near threshold, that might be expected if CDW depinning were a dynamic critical phenomenon. One possibility is that the critical regime is confined to a very small region ($\ll 0.1E_T$) around threshold and that the response outside is linear. Another possibility is that the experimental samples are too small so that the critical regime is removed by finite size effects. The observed polarization magnitude near E_T of 20 deg—a factor of 10 larger than obtained in previous NMR measurements [15]—is much more plausibly consistent with a largely elastic CDW depinning. The feasibility of NMR spectroscopy

copy on individual NbSe₃ crystals creates new opportunities for precision studies of local CDW dynamics. New simulations of realistic elastic models could allow detailed comparison of predicted phase distributions with experiment, and more carefully quantify any critical behavior in the pinned state just below E_T .

This work was carried out with support from the NSF under Grants No. DMR-0520552 (S.B.), No. DMR-0334869 (W.G.C.), and No. DMR-04-05500 (R.E.T.). P.M. thanks the Regents of the University of California and the UCLA Department of Physics and Astronomy for their hospitality.

-
- [1] P. Monceau *et al.*, Phys. Rev. Lett. **37**, 602 (1976).
 - [2] G. Grüner, Rev. Mod. Phys. **60**, 1129 (1988).
 - [3] R. M. Fleming and C. C. Grimes, Phys. Rev. Lett. **42**, 1423 (1979).
 - [4] H. Fukuyama and P. A. Lee, Phys. Rev. B **17**, 535 (1978).
 - [5] P. A. Lee and T. M. Rice, Phys. Rev. B **19**, 3970 (1979).
 - [6] D. S. Fisher, Phys. Rev. B **31**, 1396 (1985).
 - [7] O. Narayan and D. S. Fisher, Phys. Rev. B **48**, 7030 (1993).
 - [8] A. A. Middleton and D. S. Fisher, Phys. Rev. B **47**, 3530 (1993).
 - [9] C. R. Myers *et al.*, Phys. Rev. B **47**, 11171 (1993).
 - [10] A. B. Kolton *et al.*, Phys. Rev. Lett. **97**, 057001 (2006).
 - [11] S. N. Coppersmith, Phys. Rev. Lett. **65**, 1044 (1990).
 - [12] L. Balents and M. P. A. Fisher, Phys. Rev. Lett. **75**, 4270 (1995).
 - [13] L.-W. Chen *et al.*, Phys. Rev. B **54**, 12798 (1996).
 - [14] K. Saunders *et al.*, Phys. Rev. B **70**, 024205 (2004).
 - [15] J. H. Ross *et al.*, Phys. Rev. Lett. **56**, 663 (1986).
 - [16] J. H. Ross *et al.*, Phys. Rev. B **41**, 2722 (1990).
 - [17] R. E. Thorne *et al.*, Phys. Rev. B **37**, 10055 (1988).
 - [18] P. Ségransan *et al.*, Phys. Rev. Lett. **56**, 1854 (1986).
 - [19] A. Jánossy *et al.*, Phys. Rev. Lett. **59**, 2348 (1987).
 - [20] J. Shi and J. H. Ross, Phys. Rev. B **45**, 8942 (1992).
 - [21] W. H. Wong *et al.*, Phys. Rev. Lett. **72**, 2640 (1994).
 - [22] J. McCarten *et al.*, Phys. Rev. B **46**, 4456 (1992).
 - [23] J. A. Wilson, Phys. Rev. B **19**, 6456 (1979).
 - [24] F. Devreux, J. Phys. (Paris) **43**, 1489 (1982).
 - [25] S. Suh *et al.*, (unpublished).
 - [26] J. D. Kulick and J. C. Scott, Solid State Commun. **32**, 217 (1979).
 - [27] R. M. Fleming *et al.*, Phys. Rev. B **18**, 5560 (1978).
 - [28] S. N. Coppersmith, Phys. Rev. Lett. **57**, 1191 (1986).